Combined Inhibition of Smoothened and the DNA Damage Checkpoint WEE1 Exerts Antitumor Activity in Cholangiocarcinoma

Giulia Anichini[1], Chiara Raggi[2], Mirella Pastore[2], Laura Carrassa[1], Luisa Maresca[1], Enrica Crivaro[1], Tiziano Lottini[2], Lea Duwe[3], Jesper B. Andersen[3], Lorenzo Tofani[4], Luca Di Tommaso[5,6], Jesus M. Banales[7,8,9,10], Annarosa Arcangeli[2], Fabio Marra[2], and Barbara Stecca[1]

ABSTRACT

Cholangiocarcinoma (CCA) is characterized by resistance to chemotherapy and a poor prognosis. Therefore, treatments that can effectively suppress tumor growth are urgently needed. Aberrant activation of hedgehog (HH) signaling has been implicated in several cancers, including those of the hepatobiliary tract. However, the role of HH signaling in intrahepatic CCA (iCCA) has not been completely elucidated. In this study, we addressed the function of the main transducer Smoothened (SMO) and the transcription factors (TFs) GLI1 and GLI2 in iCCA. In addition, we evaluated the potential benefits of the combined inhibition of SMO and the DNA damage kinase WEE1. Transcriptomic analysis of 152 human iCCA samples showed increased expression of *GLI1, GLI2*, and Patched 1 (*PTCH1)* in tumor tissues compared with nontumor tissues. Genetic silencing of SMO, GLI1, and GLI2 inhibited the growth, survival, invasiveness, and self-renewal of iCCA cells. Pharmacologic inhibition of SMO reduced iCCA growth and viability *in vitro*, by inducing double-strand break DNA damage, leading to mitotic arrest and apoptotic cell death. Importantly, SMO inhibition resulted in the activation of the G_2–M checkpoint and DNA damage kinase WEE1, increasing the vulnerability to WEE1 inhibition. Hence, the combination of MRT-92 with the WEE1 inhibitor AZD-1775 showed increased antitumor activity *in vitro* and in iCCA xenografts compared with single treatments. These data indicate that combined inhibition of SMO and WEE1 reduces tumor burden and may represent a strategy for the clinical development of novel therapeutic approaches in iCCA.

Introduction

Cholangiocarcinoma (CCA) is an aggressive cancer of the biliary tree, and its incidence is increasing worldwide (1). The aggressive properties of this cancer are associated with the development of an abundant desmoplastic stroma, which contains high amounts of cancer-associated fibroblasts, immune cell subsets, and extracellular matrix (2, 3). Patients with CCAs are usually asymptomatic in the early stages and are often diagnosed at late stages when the therapeutic options are limited, leading to poor prognosis (4). Thus, there is an urgent need for novel and effective treatments.

The hedgehog (HH) signaling plays a pivotal role in liver regeneration and in maintaining the number of hepatic progenitors throughout life (5). It is also involved in the expansion of ductal cell populations after biliary injury (6). HH signaling is initiated through the binding of HH ligands to the 12-pass transmembrane receptor Patched 1 (PTCH1). This binding removes the repression of the 7-pass transmembrane G-protein–coupled receptor Smoothened (SMO), the main transducer of the HH pathway. Active SMO initiates an intracellular signaling cascade that ultimately leads to the activation of the zinc-finger transcription factor (TF) GLI2, which translocates to the nucleus and transactivates *GLI1* (7). Aberrant activation of HH signaling has been reported in different types of cancer (8). Several small molecule inhibitors targeting SMO have been developed, and two (vismodegib/GDC-0449 and sonidegib/LDE-225) have been approved for use in advanced basal cell carcinoma (9, 10). However, the clinical use of these SMO antagonists has been challenged by the development of resistance, severe adverse effects, and relapse upon drug withdrawal. Inhibition of HH signaling in cancer cells has been associated with the induction of DNA damage through activation of the ATM–CHK2 and ATR–CHK1 axes (11–13). These findings suggest that HH pathway inhibitors should be mechanistically

[1]Core Research Laboratory – Institute for Cancer Research and Prevention (ISPRO), Florence, Italy. [2]Department of Experimental and Clinical Medicine, University of Florence, Florence, Italy. [3]Biotech Research and Innovation Centre (BRIC), Dept. of Health and Medical Sciences, University of Copenhagen, Copenhagen, Denmark. [4]Department of Statistics, University of Florence, Florence, Italy. [5]Pathology Department, Humanitas Clinical and Research Center - IRCCS, Rozzano, Milan, Italy. [6]Department of Biomedical Sciences, Humanitas University, Pieve Emanuele, Milan, Italy. [7]Department of Liver and Gastrointestinal Diseases, Biodonostia Health Research Institute - Donostia University Hospital, University of the Basque Country (UPV/EHU), San Sebastian, Spain. [8]National Institute for the Study of Liver and Gastrointestinal Diseases (CIBERehd, "Instituto de Salud Carlos III"), Madrid, Spain. [9]Research Institute for Medicines (iMed.ULisboa), Faculty of Pharmacy, Universidade de Lisboa, Lisbon, Portugal. [10]Department of Biochemistry and Genetics, School of Sciences, University of Navarra, Pamplona, Spain.

Current address for G. Anichini: Department of Biomedical, Experimental and Clinical Sciences "Mario Serio", University of Florence, Florence, Italy.

G. Anichini and C. Raggi contributed equally to this article.

Corresponding Authors: Barbara Stecca, Core Research Laboratory – Institute for Cancer Research and Prevention (ISPRO), Viale Pieraccini 6, Florence 50139, Italy. Phone: +39-55-794-4567; E-mail: b.stecca@ispro.toscana.it; and Fabio Marra, Department of Experimental and Clinical Medicine, University of Florence, Largo Brambilla 3, Florence 50134, Italy. Phone: +39-55-794-5425; E-mail: fabio.marra@unifi.it

Mol Cancer Ther 2023;22:343–56

doi: 10.1158/1535-7163.MCT-22-0379

combined with replication-associated DNA-damaging agents to potentiate antitumor activity.

Previous reports have highlighted the requirement of HH signaling for the growth, proliferation, and survival of CCA (14–19). However, most of these studies were based on the use of cyclopamine or first-generation SMO inhibitors, and the cellular and biological functions controlled by HH signaling in intrahepatic CCA (iCCA) have not been completely elucidated. Here, we thoroughly investigated the effects of pharmacologic and genetic inhibition of HH signaling in iCCA. Our data revealed that targeting HH signaling at different levels reduces proliferation, invasion, and self-renewal in human iCCA cells. Interestingly, pharmacologic inhibition of SMO induced the activation of the key G_2–M and DNA damage checkpoint kinase WEE1. Combined inhibition of SMO and WEE1 with specific inhibitors resulted in a strong reduction in iCCA cell growth *in vitro* and a dramatic decrease in tumor growth *in vivo*.

Materials and Methods

Cell lines

HEK-293T (RRID: CVCL_0063) cells were purchased from ATCC (Manassas, VA). The iCCA cell lines HuCCT1 (RRID: CVCL_0324) and CCLP1 (RRID: CVCL_0205) were kindly provided by Dr. A.J. Demetris, University of Pittsburgh, and the primary culture of normal human cholangiocytes (NHCs) by Prof. J.M. Banales (4). Cells were cultured according to previously described conditions (20). Experiments were performed within 5 weeks after defrosting cells. Cells were regularly tested for potential Mycoplasma contamination using PCR.

Gene expression analysis

Gene expression profiles were obtained from a publicly available dataset, Copenhagen, Denmark (GSE26566; ref. 21), including additional patients profiled on human Ref-8 v2.0 expression beadchip arrays (Illumina). In total, 152 human iCCA tumor samples and 143 matched tumor-adjacent normal liver samples were analyzed. The Institutional Review Board approval was provided by the contributing local departments in compliance with the Declaration of Helsinki. Written informed consent was obtained from all patients (21). Differential analysis was performed on log2 transformed data comparing the tumors with the surrounding normal tissues.

Drugs and treatments

LDE-225 (sonidegib; ref. 22) and GANT61 (23) were purchased from Selleckchem (Munich, Germany). The SMO inhibitors MRT-92 (EPMF03 or Compound 1) and EPMF11 (or Compound 2) were previously described (13, 24). The WEE1 inhibitor AZD-1775 (MK-1775, adavosertib; ref. 25) was provided by MedChemExpress (Monmouth Junction, NJ). Nocodazole was purchased from Sigma-Aldrich (St. Louis, MO) and used at a concentration of 600 nmol/L for 16 hours.

For dose–response curves, 25×10^3 cells/well HuCCT1 and CCLP1 cells were treated with increasing concentrations of each compound in reduced-serum medium (1% FBS) for 72 hours. Cells were fixed with 4% paraformaldehyde, stained with crystal violet, and absorbance was measured with a VICTOR X5 (Multilabel Plate Reader, PerkinElmer). The curves were obtained using GraphPad Prism 6 (RRID: SCR_000306).

Lentiviral vectors and plasmids

Lentiviral particles were produced in HEK-293T cells as previously described (26). The short hairpin RNA (shRNA) vectors used were: pLKO.1-puro (scramble, LV-c; (RRID: Addgene_8453), pLKO.1-puro-shSMO (targeting sequence 5′- GTGGAGAAGAT-CAACCTGTTT-3′), pLKO.1-puro-shGLI1 (targeting sequence 5′-CATCCATCACAGATCGCATTT-3′; ref. 27), pLKO.1-puro-shGLI2 (targeting sequence 5′- CCGCTTCAGATGACAGATGTT-3′; ref. 28), pLKO.1-puro-shWEE1–704 (targeting sequence 5′- GCCAGTGAT-TATGAGCTTGAA-3′), and pLKO.1-puro-shWEE1–424 (targeting sequence 5′- TTCTCATGTAGTTCGATATTT-3′). All sequences were obtained from Open Biosystems (Lafayette, CO) and validated in previous studies using a second independent shRNA for each gene (27, 28).

Growth curves and colony-formation assay

For the growth curve, transduced HuCCT1 and CCLP1 cells were seeded (9×10^3 cells/well) and on days 0, 3, 5, and 7, cells were fixed with 4% paraformaldehyde, stained with crystal violet, and absorbance was measured with VICTOR X5 (Multilabel Plate Reader, PerkinElmer). For colony-formation assay, transduced HuCCT1 and CCLP1 cells were seeded at a low density (700 cells/well) in complete medium. On days 10 to 15, cells were fixed and stained with crystal violet, and colonies were counted using the ImageJ software.

Invasion and self-renewal assays

Invasion was measured in a modified Boyden chamber equipped with 8 μmol/L pore filters (Millipore Corp,) coated with Matrigel (150 μg/mL; BD Biosciences) as previously described (29). After incubation at 37°C (24 hours), cells that invaded the underside of the filters were fixed and stained with Giemsa. Invasion assay was expressed as the average number of invading cells per microscopic field (40×) over at least five fields.

For self-renewal assay, five hundred iCCA cells were grown under anchoring-independent conditions in poly 2-hydroxyethyl methacrylate (poly-HEMA)-coated dishes (Sigma-Aldrich) with serum-free DMEM/F12 medium supplemented with 1X B27 without vitamin A (Life Technologies), 20 ng/mL EGF, and 20 ng/mL bFGF (R&D Systems; refs. 30, 31). After 7 days, images were taken to measure the number and size of spheres using a Leica DMi1 microscope (Leica). The average number of formed spheres was determined in a microscopic field (20×) over at least five fields.

Caspase 3/7 activity assay

Following treatments, Caspase-Glo 3/7 Assay (Promega) kit was used to measure the activity of cleaved caspase-3 and -7 in whole cell lysate. Fifteen μg of protein samples in 25 μL total volume was mixed with equal volume (25 μL) of Caspase-Glo reagent and incubated at room temperature for 30 minutes. Then, the luminescence was measured using GloMax 20/20 Luminometer (Promega).

Western blot

For Western blot, cells were lysed in cold RIPA buffer (1% NP-40, 150 mmol/L NaCl, 5 mmol/L EDTA, 0,25% NaDOC, 50 mmol/L Tris-HCL pH 7.5, 0,1% SDS) supplemented with protease and phosphatase inhibitors and processed as previously described (26). The primary antibodies used are summarized in Supplementary Table S1.

Immunofluorescence

HuCCT1 and CCLP1 cells were treated with MRT-92, fixed with 4% paraformaldehyde, and incubated in blocking solution (2% BSA in 0.2% PBS-Triton). Primary anti-pSer10 histone H3 antibody (Cell Signaling Technology) and secondary Alexa Fluor 488 goat anti-rabbit IgG (Thermofisher) were used. Nuclei were stained with DAPI, and

samples were observed with an Axio Observed Z1 inverted microscope (Zeiss). Prophase nuclei were counted using ImageJ and normalized to total DAPI counts.

Flow cytometric analysis

For cell-cycle analysis, iCCA cells were fixed and stained with propidium iodide (50 μg/mL) and ribonuclease (5 U/mL). Data were recorded using CytoFLEX S (BD Beckman Coulter), and the results were analyzed using ModFit LT software (Verity Software House, (RRID: SCR_016106). For the mitotic synchronization, iCCA cells were treated with nocodazole 600 nmol/L for 16 hours, and then treated with MRT-92 in medium containing 1% FBS at the indicated doses for 36 hours. Cell-cycle distribution was analyzed by FACS every 2 hours. Apoptosis was analyzed using the Annexin V/7-AAD Apoptosis Kit (BD Biosciences, San Jose, CA), according to the manufacturer's instructions. The percentages of both early (Annexin V+/7-AAD−) and late (Annexin V+/7-AAD+) apoptotic cells were detected and measured using CytoFLEX S (BD Beckman Coulter).

CCA xenografts

CCLP1 cells were resuspended in Matrigel (Sigma)/DMEM (1/1) and injected subcutaneously into the right lateral flank of adult (8 weeks) male NOD/SCID mice (Charles River Laboratories; 4×10^6 cells/injection). Once tumors were 100 mm^3 on average, mice were randomized into four groups and treated intraperitoneally with MRT-92 (20 mg/kg, twice a day), by gavage with AZD-1775 (50 mg/kg, once a day), combination of MRT-92 and AZD-1775, or vehicle for 19 days, following 6 days on/1 day off treatment schedule. MRT-92 was dissolved in 20% 2-hydroxypropyl-β-cyclodextrin (Sigma-Aldrich), whereas AZD-1775 was dissolved in 0.5% methylcellulose (Sigma-Aldrich), kept in the dark with continuous stirring, and freshly prepared every 4 days. Vehicle mice were treated with 20% 2-hydroxypropyl-β-cyclodextrin intraperitoneally (twice a day) and with 0.5% methylcellulose via gavage (every day). The subcutaneous tumor size was measured weekly using ultrasound and photoacoustic imaging (Vevo). The health status of mice was assessed by measuring their body weight once a week. The mice were fed with a standard rodent chow diet *ad libitum*. For pharmacodynamic studies, tumor-bearing mice were treated with drugs or vehicle for 3 days. Animals were euthanized 3 hours after the last treatment, and the tumors were dissected and snap-frozen. Frozen specimens were homogenized in protein lysis buffer, loaded on SDS-PAGE, and immunoblotted with specific antibodies. All procedures were conducted in accordance with the Animal Ethical Committee of the Italian Ministry of Health (authorization No. 412/2021-PR).

Ultrasound and photoacoustic imaging (Vevo)

Mice were anesthetized with isoflurane (induction dose at 4% and maintenance dose at 2%) and placed on a heated pad (37°C) in the prone position, and ECG, respiration rate, and body temperature were steadily monitored. An ultrasound transmission gel was applied to mouse skin for an efficient transduction of ultrasound and photoacoustic signals. Photoacoustic and ultrasound imaging were performed using a Vevo LAZR-X system (Fujifilm VisualSonics). Axial 3D scans of the tumor masses were performed using B-Mode imaging with a 55-MHz transducer. The volumes were subsequently measured by delineating the region of interest for each axial slide using the Vevo LAB software. For photoacoustic imaging, a Vevo Optical Fiber (Silica fiber, Narrow) was placed on a Vevo Fiber Jacket positioned on the transducer. Photoacoustic acquisitions were performed at 750 nm and 850 nm to obtain parametric maps of SO_2.

IHC

IHC was performed in formalin-fixed, paraffin-embedded section of CCLP1 xenografts. After antigen retrieval (with citrate buffer pH 6.0), staining was performed with the UltraVision Detection System Kit (Lab Vision, Fremont, CA) following the manufacturer's instructions. Sections were incubated overnight at 4°C with rabbit anti-cleaved caspase 3 antibody (RRID: AB_10897512). DAB (Dako, Copenhagen, Denmark) was used as chromogen. Nuclei were counterstained with hematoxylin.

Statistical analysis

Data represent mean ± SD or ± SEM values calculated on at least three independent experiments. No statistical methods were used for the sample size selection. *P* values were calculated using Student *t* test (two groups) or one-way ANOVA (more than two groups). Statistical significance of the *in vivo* experiment was assessed using Welch ANOVA and Games-Howell test for multiple comparisons. Differences were considered statistically significant at *, $P < 0.05$; **, $P < 0.01$; ***, $P < 0.001$; ****, $P < 0.0001$.

Data availability

All the data generated during this study are included in this article and its online supplementary material. Further inquiries can be directed to the corresponding authors.

Results

The HH pathway is upregulated in iCCA

To analyze the involvement of the HH pathway in iCCA, we first tested the expression levels of the TFs *GLI1* and *GLI2*, and the target *PTCH1*, the best read-out of an active HH pathway. Bioinformatics analysis of transcriptomic datasets from 152 surgically resected human iCCA samples showed increased expression of *GLI1, GLI2*, and *PTCH1* in the tumor compared with the matched surrounding nontumor tissue (**Fig. 1A**). Consistently, Western blot analysis showed that GLI1 and GLI2 were expressed at higher levels in HuCCT1 and CCLP1 iCCA cell lines than in NHCs (Supplementary Fig. S1). In particular, CCLP1 cells expressed higher levels of GLI1 protein than GLI2, whereas HuCCT1 cells displayed a preferential expression of GLI2. Interestingly, both iCCA cell lines displayed high levels of the transmembrane receptor SMO, which is the main druggable target of the HH pathway. These data indicate that the HH pathway is active in iCCA tumors and cell lines, as previously reported (16, 32).

Genetic silencing of SMO, GLI1, and GLI2 negatively affects iCCA cell proliferation, invasion and self-renewal

Transcriptome data on human iCCAs and matched tumor-adjacent normal tissues suggest a possible role of the HH signaling in iCCA, presenting a significant upregulation of *GLI1* and *GLI2* in the tumors. Therefore, we investigated the involvement of the HH pathway in iCCA. SMO and the TFs GLI1 and GLI2 were silenced using lentiviral vectors (LVs) encoding specific shRNAs (27, 28), as confirmed by a strong decrease in protein expression by Western blotting (**Fig. 1B**). Silencing of SMO, GLI1, and GLI2 reduced the long-term growth at 7 days (**Fig. 1C**) and colony-formation ability (**Fig. 1D**) of both iCCA cell lines. HuCCT1 cells showed a stronger dependency on GLI1 function for growth, whereas CCLP1 were more dependent on SMO. On the other hand, colony formation was equally and significantly reduced by silencing of SMO, GLI1, or GLI2 compared with control cells (**Fig. 1D**). The decrease in iCCA cell growth induced by the

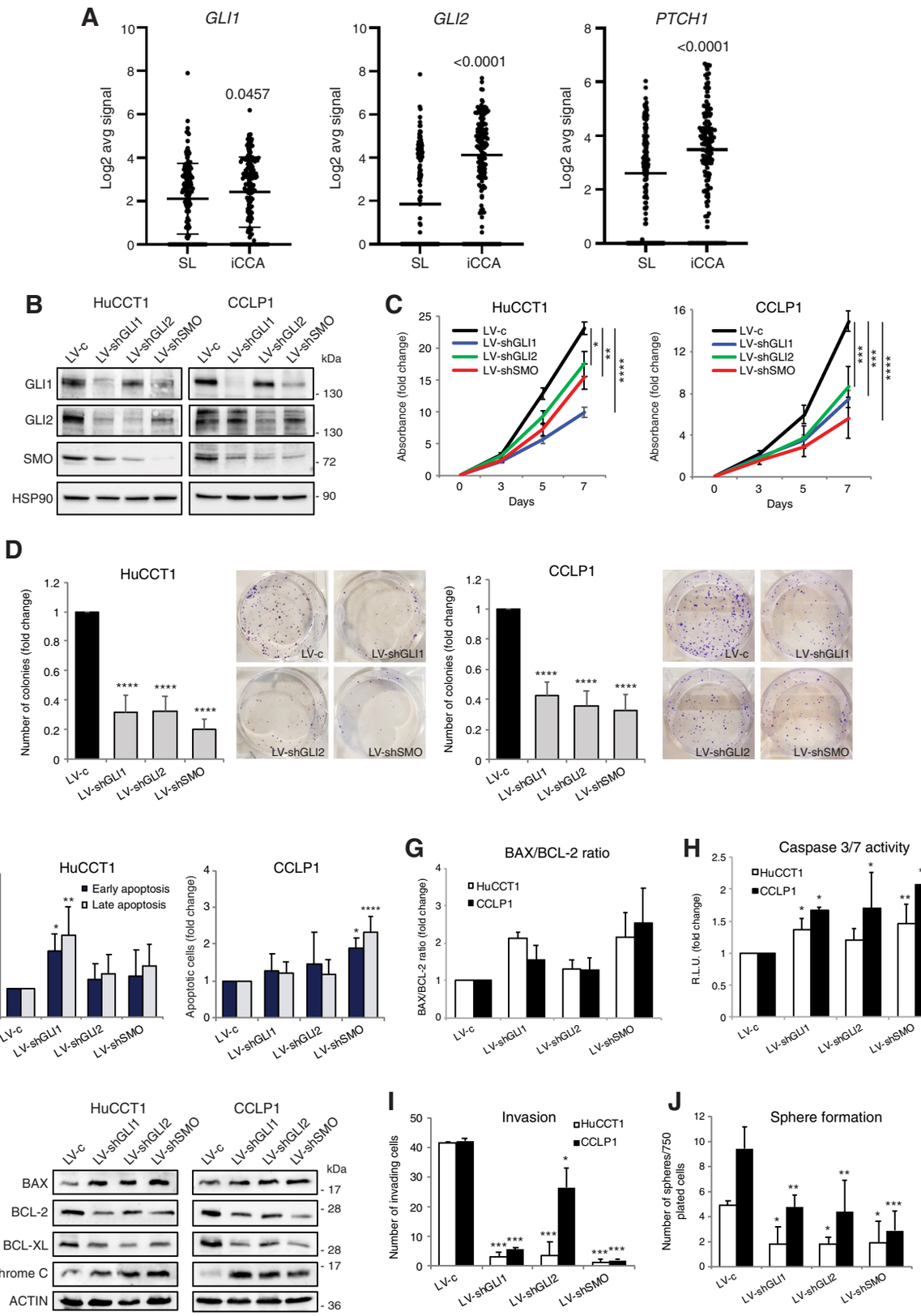

silencing of SMO, GLI1, and GLI2 was the result of an increase in apoptosis. In particular, HuCCT1 cells showed a significant increase in both early and late apoptosis upon depletion of GLI1 and, to a lesser extent, upon SMO silencing. CCLP1 cells presented a significantly increased fraction of cells in early and late apoptosis only upon SMO silencing (**Fig. 1E**). At the molecular level genetic silencing of GLI1, GLI2, and SMO increased the protein levels of BAX and cytochrome C, and decreased BCL-2 and BCL-XL expression (**Fig. 1F** and **G**). This effect was also confirmed by increased activity of Caspase 3/7 (**Fig. 1H**).

Genetic silencing of SMO, GLI1, and GLI2 drastically decreased other malignant features in both cell lines. Invasion of HuCCT1 and CCLP1 cells was strongly reduced by SMO, GLI1, or GLI2 ablation (**Fig. 1I**). Similarly, silencing of SMO, GLI1, and GLI2 significantly diminished the sphere formation ability in both cell types (**Fig. 1J**). Our results demonstrate that the HH transducer SMO and the TFs GLI1 and GLI2 are critical for maintaining the viability, growth, invasiveness, and self-renewal of iCCA cells.

Pharmacologic inhibition of HH pathway reduces survival and proliferation in HuCCT1 and CCLP1 cells

After validating the prosurvival function of HH signaling in iCCA cells through gene silencing, we investigated whether pharmacologic targeting of different pathway members is a feasible strategy to block iCCA cell growth. Different SMO and GLI inhibitors were tested through 72 hours dose–response curves and selected for further studies according to the IC_{50} of each compound (**Fig. 2A** and **B**; Supplementary Fig. S2). Pharmacologic inhibition of HH signaling at the level of the transmembrane receptor SMO and the downstream TFs GLI strongly reduced iCCA cell viability *in vitro*. The SMO inhibitors MRT-92 (EPMF03) and EPMF11 (13, 33) showed the lowest IC_{50} values (nanomolar to low micromolar) compared with the SMO reference compound LDE225 (22, 34) and the GLI1/2 inhibitor GANT61 (ref. 23; **Fig. 2A–C**). In particular, both SMO antagonists, MRT-92 and EPMF11, which our group recently tested in *vitro* and in orthotopic models of melanoma (13), suppressed endogenous GLI1 protein levels in a dose-dependent manner (**Fig. 2D** and **E**).

Pharmacologic blockade of SMO results in the accumulation and arrest of iCCA cells in G_2–M phase

First, we assessed whether the SMO inhibitors MRT-92 and EPMF11 affected cell-cycle distribution using propidium iodide staining and FACS analysis of HuCCT1 and CCLP1 cells treated for 72 hours with increasing concentrations of each compound. Treatment with either compound induced dose-dependent enrichment in the 4N fraction of the cell cycle, accompanied by a reduction in G_0–G_1 and an increase in G_2–M phases (**Fig. 3A** and **B**). Several compounds have been shown to function as antitumor agents by inducing DNA damage and subsequent apoptosis (35). Therefore, we investigated whether the accumulation of cells in the G_2–M phase could be dependent on the activation of cell-cycle checkpoints, as a result of the induction of DNA damage response pathways. To further investigate the mechanism underlying the observed arrest of cells in the G2 or M phase, HuCCT1 and CCLP1 cells were synchronized in prometaphase using the spindle-interfering agent nocodazole. Cells were then released in the absence or presence of increasing doses of MRT-92, and DNA content was analyzed at different time points until 36 hours of treatment. FACS analysis confirmed the arrest in the M-phase after nocodazole treatment, as shown by the 4N DNA content of cells immediately after blocking (0 hour; **Fig. 3C**). DMSO-treated iCCA cells showed an increase in the percentage of G_1 phase after 4 hours. In contrast, MRT-92–treated cells delayed their reentry into the cell cycle, and the majority of cells were arrested in the G_2–M phase until 8 hours after removal of nocodazole, suggesting a blockade of cells in G_2–M. Notably, the subG0 peak, which is an index of cell death, increased in MRT-92–treated cells between 12 and 24 hours after nocodazole release. This phenomenon suggests a failure in repairing most intracellular damages, resulting in the inability to bypass cell-cycle checkpoints and induction of cell death (**Fig. 3C**).

The SMO inhibitor MRT-92 induces double-strand break DNA damage and activates WEE1

Treatment with MRT-92 arrested iCCA cells in the G_2–M phase, due to the induction of double-strand break (DSB) DNA damage, as shown by increased phosphorylation of histone γH2A.X (36) and dose-dependent induction of the DNA damage sensor PARP1 (**Fig. 3D**). Consequently, MRT-92 promoted the activation and phosphorylation of ATM (Ser1981), one of the main initiators of the DNA damage response following DSB and its direct target CHK2 (Thr68; **Fig. 3D**). CHK2 is implicated in both the G1/S and G_2–M checkpoints (37). However, propidium iodide staining and molecular analysis ruled out the possibility that MRT-92 induces G_1–S arrest because decreased Cyclin A2 levels indicate that treated cells are able to progress through the G_1–S checkpoint. Instead, MRT-92 treatment strongly affected the G_2–M transition. The activation of WEE1 led to the inhibitory phosphorylation of CDC2/CDK1 at Tyr15 (38), with the consequent accumulation of Cyclin B1, compromising the ability of cells to progress through mitosis (**Fig. 3E**). Nevertheless, the dose-dependent increase in the levels of the mitotic marker pSer10-histone H3 (39) suggests that cells are able to initiate the very early phases of mitosis. However, Cyclin B1 was not degraded (40), indicating that iCCA cells failed to complete cell division owing to the inability to repair MRT-92–induced DNA damage (**Fig. 3E**). Consistently, pSer10-histone H3 immunofluorescence revealed that treatment with MRT-92 arrested iCCA cells in early prophase (**Fig. 4A** and **B**).

Figure 1.

HH pathway is required for iCCA cell proliferation, invasion and stemness. **A,** *GLI1, GLI2*, and *PTCH1* mRNA expression in human iCCA tissue ($n = 152$) compared with matched normal liver tissue (SL; $n = 143$) using transcriptome data. **B,** Western blot of GLI1, GLI2, and SMO in HuCCT1 and CCLP1 cells transduced with LV-c, LV-shGLI1, LV-shGLI2, or LV-shSMO. HSP90 was used as loading control. **C,** Long-term growth curves in HuCCT1 and CCLP1 cells transduced as indicated. **D,** Colony assay in HuCCT1 and CCLP1 cells transduced as indicated. **E,** Evaluation of cellular apoptosis by AnnexinV/7-AAD double staining in HuCCT1 and CCLP1 cells transduced as indicated. Early apoptosis is detected by Annexin V+/7-AAD-, late apoptosis by Annexin V+/7-AAD+. **F,** Western blot of apoptotic markers in HuCCT1 and CCLP1 cells transduced as indicated. ACTIN was used as loading control. **G,** Densitometric quantification of BAX/BCL-2 ratio in HuCCT1 and CCLP1 cells transduced as indicated in E. **H,** Activity of caspase 3 and 7 in HuCCT1 and CCLP1 cells transduced with LV-c, LV-shGLI1, LV-shGLI2, or LV-shSMO. **I,** Invasion assay in HuCCT1 and CCLP1 cells transduced as indicated. **J,** Sphere formation assay in HuCCT1 and CCLP1 cells transduced as indicated. In **D–H,** data are expressed as fold change relative to control (LV-c), which was equated to 1. Data represent mean ± SD of at least three independent experiments. *, $P < 0.05$; **, $P < 0.01$; ***, $P < 0.001$; ****, $P < 0.0001$.

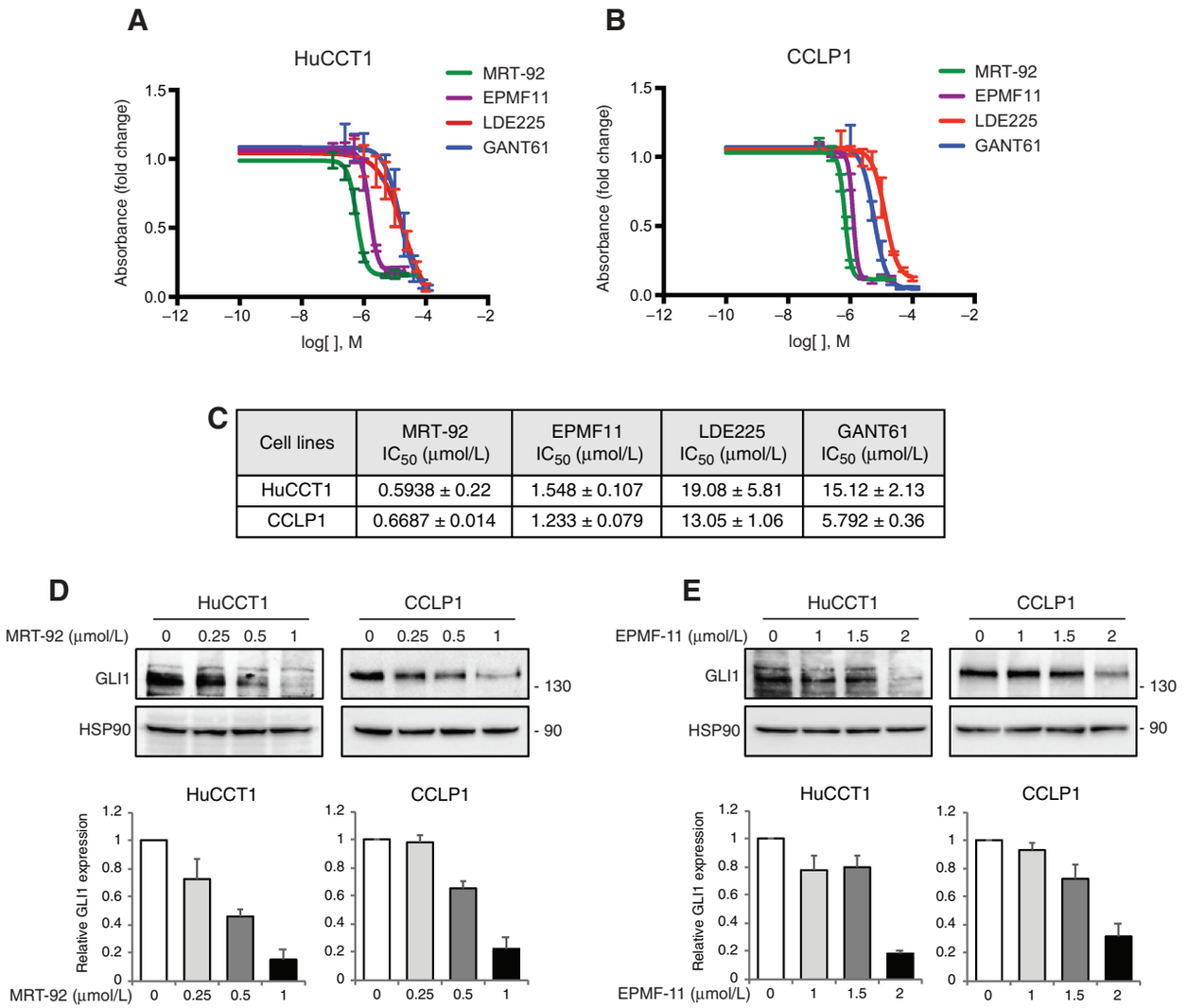

Cell lines	MRT-92 IC_{50} (μmol/L)	EPMF11 IC_{50} (μmol/L)	LDE225 IC_{50} (μmol/L)	GANT61 IC_{50} (μmol/L)
HuCCT1	0.5938 ± 0.22	1.548 ± 0.107	19.08 ± 5.81	15.12 ± 2.13
CCLP1	0.6687 ± 0.014	1.233 ± 0.079	13.05 ± 1.06	5.792 ± 0.36

Figure 2.

Pharmacologic inhibition of HH pathway suppresses iCCA cell viability and growth in a dose-dependent manner. **A** and **B,** Dose–response curves of MRT-92, EPMF11, LDE-225 (SMO inhibitors), and GANT-61 (GLI1/2 inhibitor) in HuCCT1 (**A**) and CCLP1 (**B**) cells treated for 72 hours with DMSO or increasing doses of each compound. Data are expressed as fold change relative to DMSO, which was equated to 1. Curves were obtained using GraphPad Prism 6. **C,** Table reports IC_{50} values for each cell line. **D,** Western blot analysis and densitometric quantification of GLI1 in HuCCT1 and CCLP1 cells treated for 72 hours with DMSO or increasing doses of MRT-92. **E,** Western blot analysis and densitometric quantification of GLI1 in HuCCT1 and CCLP1 cells treated for 72 hours with DMSO or increasing doses of EPMF11. HSP90 was used as loading control. Data represent mean ± SD of at least three independent experiments.

Pharmacologic inhibition of SMO results in the induction of apoptosis

AnnexinV/7-AAD double staining revealed a strong proapoptotic effect of SMO pharmacologic inhibition in iCCA. FACS analysis showed a significant dose-dependent increase in both early and late apoptosis in the presence of either SMO antagonists MRT-92 or EPMF11 (**Fig. 5A** and **B**). In particular, MRT-92 treatment reduced the expression of the antiapoptotic proteins BCL-XL and BCL-2, leading to the release of cytochrome C, induction of cleaved caspase 3, and increased activity of caspase 3/7 (**Fig. 5C–E**), together with PARP1 cleavage (**Fig. 3D**). Altogether, these data indicate that MRT-92–dependent activation of ATM–CHK2 checkpoint arrested cells before the finalization of mitosis, leading to programmed mitochondrial cell death.

Targeting the cell-cycle checkpoint kinase WEE1 enhances the effect of SMO inhibition in reducing iCCA growth

The above data demonstrated that MRT-92 treatment induces WEE1 phosphorylation at Ser642 in both iCCA cell lines (**Fig. 3E**), leading to its activation (41, 42). WEE1 is a critical cell-cycle checkpoint kinase involved in the DNA damage response and cell-cycle regulation. Several lines of evidence suggest that WEE1 upregulation exerts protumorigenic activity, making cancer cells less sensitive to genomic instability. Thus, several WEE1 inhibitors are currently under investigation as anticancer therapeutics (43). Therefore, we reasoned that the inhibition of WEE1 could exacerbate the accumulation of damaged DNA induced by MRT-92, enhancing the effect of SMO inhibition. Treatment with the WEE1 inhibitor AZD-1775 potentiated the proapoptotic and antiproliferative effects of MRT-92 in both cell

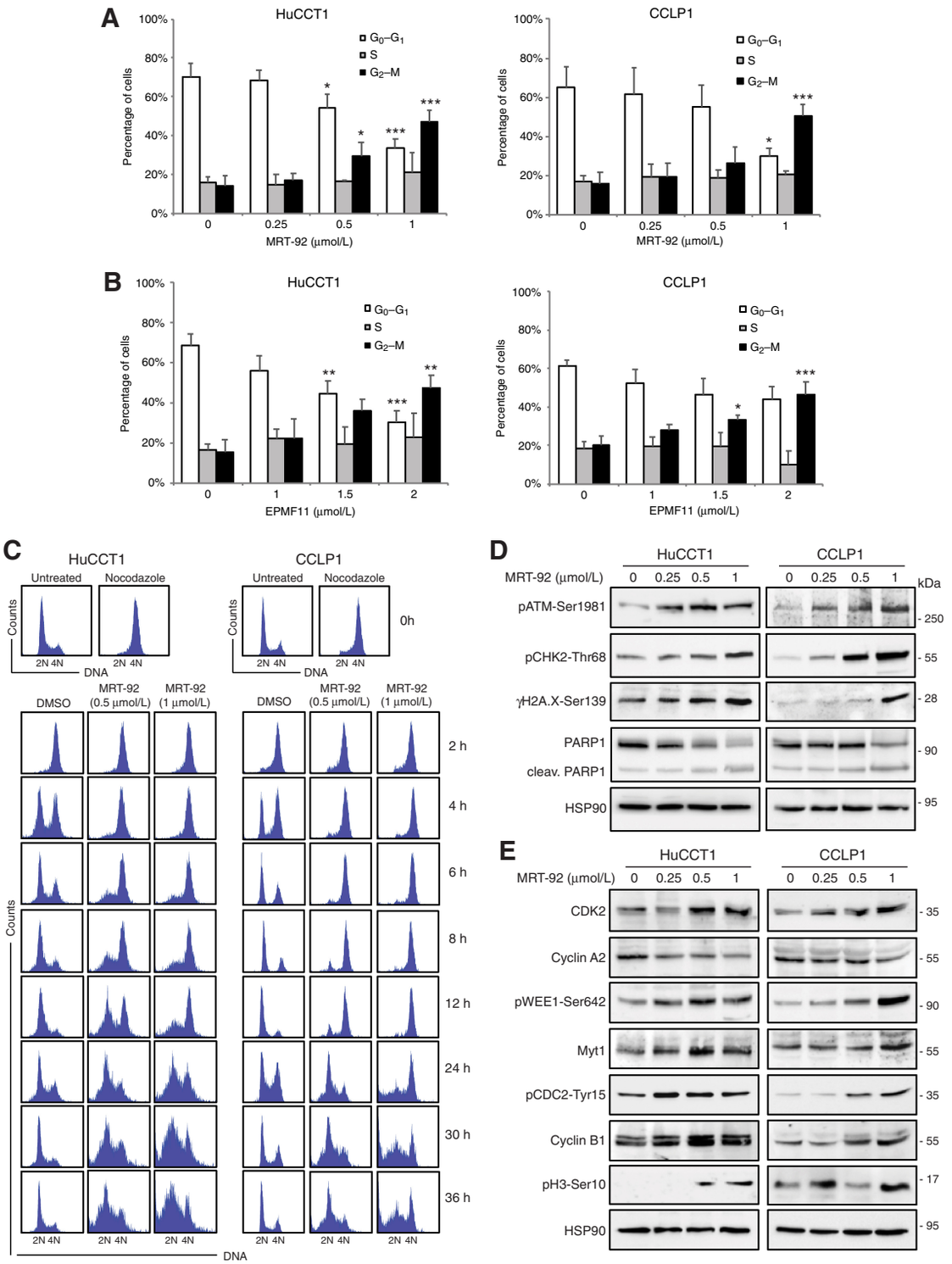

Figure 3.

SMO inhibition using MRT-92 induces DNA damage. **A** and **B,** Cell-cycle analysis of HuCCT1 and CCLP1 cells treated for 72 hours with DMSO or increasing doses of MRT-92 and EPMF11. **C,** Effect of nocodazole treatment (600 nmol/L) for 16 hours in HuCCT1 and CCLP1 cells. Cells were treated with DMSO or increasing doses of MRT-92 after release from nocodazole block and cell-cycle distribution was determined by flow cytometric analysis after propidium iodide staining. **D** and **E,** Western blot of DNA damage (**D**) and cell-cycle markers (**E**) in HuCCT1 and CCLP1 cells treated for 72 hours with DMSO or increasing doses of MRT-92. HSP90 was used as loading control. Data represent mean ± SD of at least three independent experiments. *, $P < 0.05$; **, $P < 0.01$; ***, $P < 0.001$.

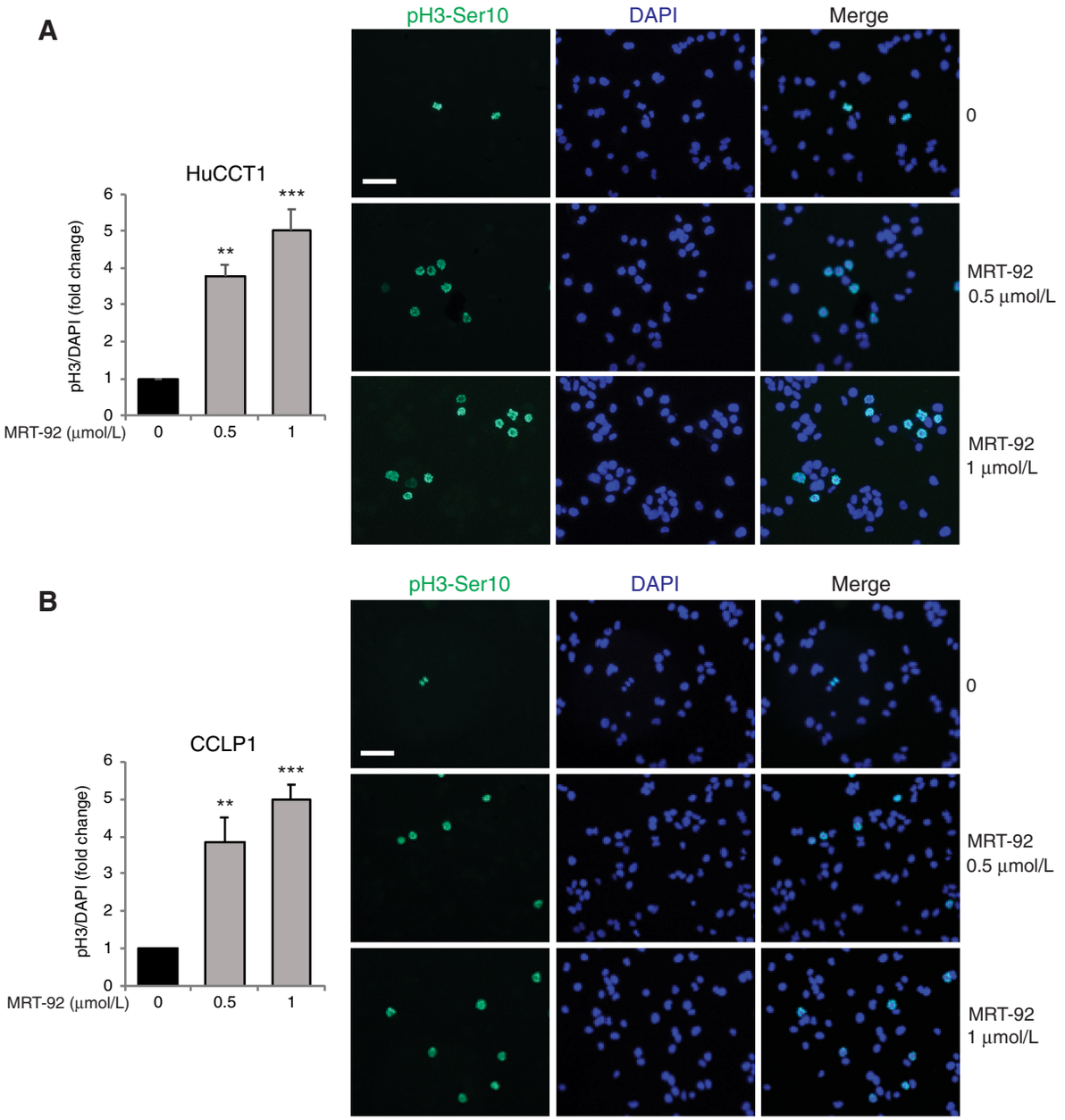

Figure 4.

The SMO inhibitor MRT-92 arrests iCCA cells at early prophase of mitosis. **A** and **B,** Immunofluorescence of pH3-Ser10 in HuCCT1 (**A**) and CCLP1 (**B**) cells treated for 16 hours with DMSO or MRT-92 (0.5, 1 μmol/L). Data are expressed as fold change relative to DMSO, which was equated to 1. Nuclei were counted with ImageJ and histograms report FITC/DAPI ratio. Data represent mean ± SD of at least three independent experiments. Scale bar = 100 μm. **, $P < 0.01$; ***, $P < 0.001$.

lines, particularly in CCLP1 cells (**Fig. 6A** and **B**). The combination of both inhibitors produced a strong reduction in iCCA cell viability and growth already at 24 hours, whereas single treatments showed effects only at later time points (**Fig. 6A** and **B**). To assess the specificity of AZD-1775, WEE1 was silenced using two independent shRNAs. Both abrogated WEE1 protein levels in both iCCA cell lines and reduced phosphorylation of CDC2 on Tyr15, indicating that depletion of WEE1 has the same inhibitory activity of the WEE1 inhibitor AZD-1775 (Supplementary Fig. S3A). Long-term growth curves showed that genetic silencing of WEE1 produces the same effect of AZD-1775 in reducing cell viability (Supplementary Fig. S3B). In addition, treatment with MRT-92 in WEE1-silenced iCCA cells mimics the effect of the pharmacologic combination of MRT-92 + AZD-1775 (Supplementary Fig. S3C), suggesting the specificity of AZD-1775 at the doses used in this study.

At the molecular level, the combination treatment strongly increased the induction of DNA damage, as shown by the increased expression of γH2A.X and PARP1 cleavage compared with the single

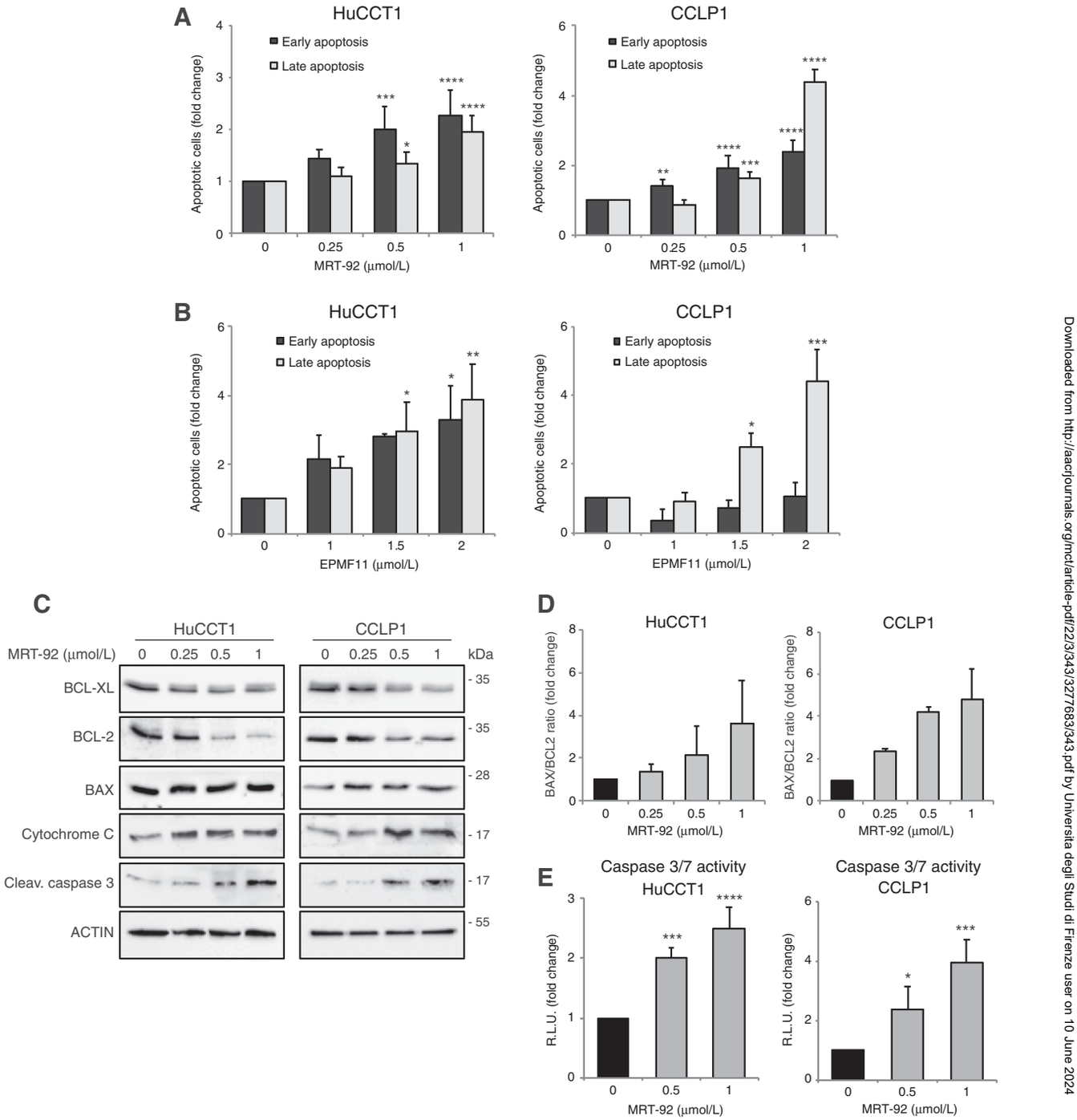

Figure 5.

SMO inhibition induces apoptosis in iCCA cells. **A** and **B,** Evaluation of apoptosis by AnnexinV/7-AAD double staining in HuCCT1 and CCLP1 cells treated for 72 hours with DMSO or increasing doses of MRT-92 (**A**) and EPMF11 (**B**). Early apoptosis is detected by Annexin V+/7-AAD-, late apoptosis by Annexin V+/7-AAD+. **C,** Western blot of apoptotic markers in HuCCT1 and CCLP1 cells treated for 72 hours with DMSO or increasing doses of MRT-92. ACTIN was used as loading control. **D,** Densitometric quantification of BAX/BCL-2 ratio in HuCCT1 and CCLP1 cells treated as indicated in **(C)**. **E,** Activity of caspase 3 and 7 in HuCCT1 and CCLP1 cells treated as indicated. In **A, B**, **D,** and **E,** data are expressed as fold change relative to DMSO, which was equated to 1. Data represent mean ± SD of at least three independent experiments. *, $P < 0.05$; **, $P < 0.01$; ***, $P < 0.001$; ****, $P < 0.0001$.

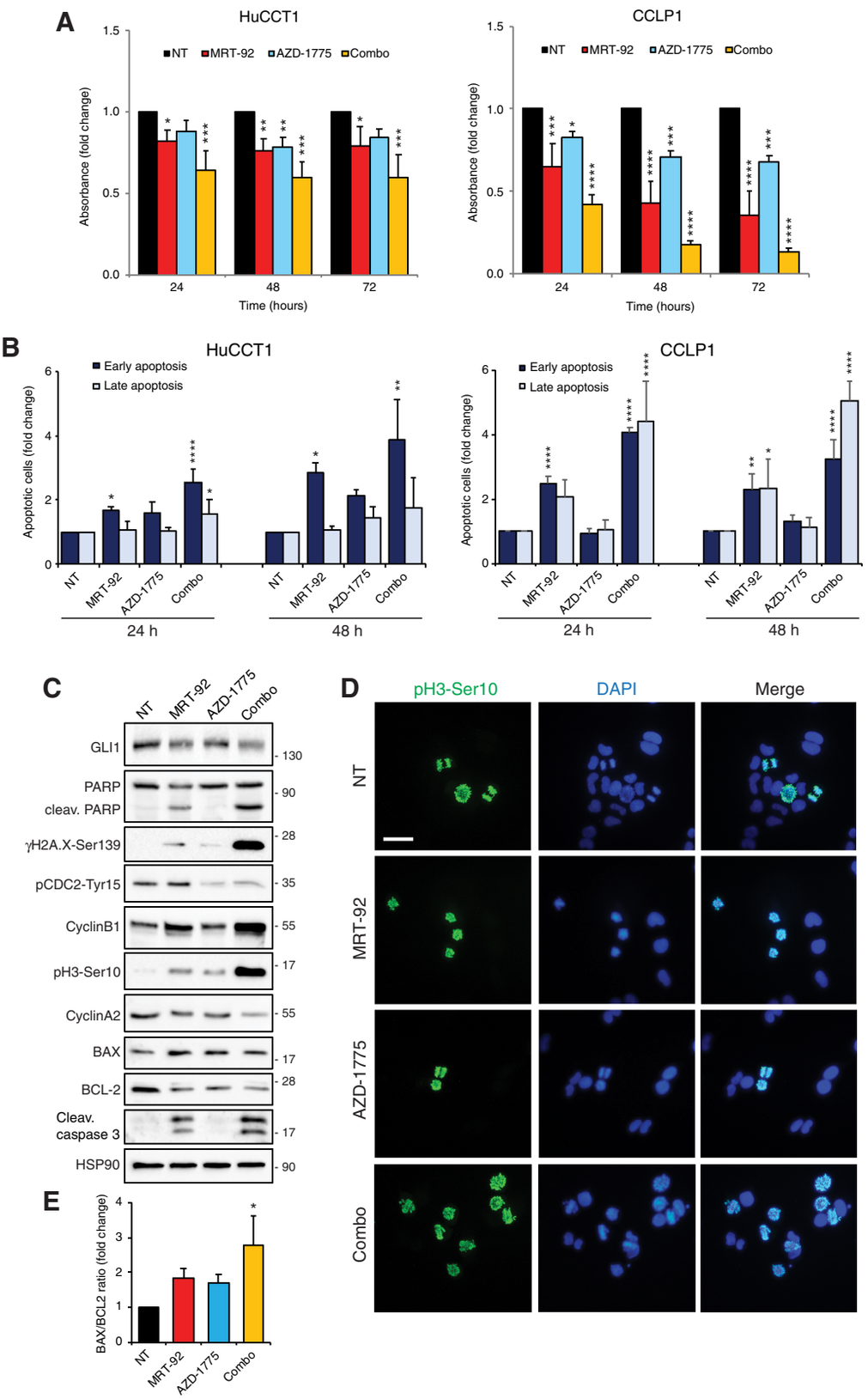

treatments (**Fig. 6C**). Furthermore, dual MRT-92+AZD-1775 treatment increased the arrest of cells in mitosis, as indicated by higher levels of phosphorylated H3 and enhanced accumulation of Cyclin B1, compared with single treatments (**Fig. 6C** and **D**; Supplementary Fig. S4). Immunofluorescence of pSer10-histone H3 confirmed that the WEE1 inhibitor AZD-1775 strongly worsened the degree of DNA damage induced by the SMO inhibitor MRT-92. In fact, the combination treatment strongly affected the mitotic process, as iCCA cells bypassed MRT-92-induced arrest in the early prophase. Nevertheless, cells were unable to separate replicated DNA correctly, as shown by the large presence of aberrant mitotic nuclei at both 24 and 48 hours (**Fig. 6D**; Supplementary Fig. S4). Accordingly, the subsequent failure of iCCA cells to repair DNA damage resulted in a more powerful induction of both early and late apoptosis, as indicated by the increase in the BAX/BCL-2 ratio and by the enhanced levels of cleaved caspase 3 (**Fig. 6C** and **E**).

Combined targeting of SMO and WEE1 elicits a significant antitumor activity in iCCA xenografts

The efficacy of the simultaneous SMO and WEE1 blockade was assessed in an iCCA xenograft model (**Fig. 7A**). Treatment with low doses of either AZD-1775 (T/C % 67.6) or MRT-92 (T/C % 68.5) as single agents (monotherapy) did not significantly reduce tumor growth. In contrast, the combination of AZD-1775 and MRT-92 significantly reduced tumor growth compared with that in vehicle-treated mice (T/C % 26.5) ($P < 0.0001$) or mice treated with a single agent (Combo vs. MRT-92; $P = 0.0239$; Combo vs. AZD-1775; $P = 0.0279$; **Fig. 7B**-**D**). Treatment with single agents or their combination was well tolerated, in mice and body weight was not significantly affected (**Fig. 7E**). These drugs were able to inhibit their respective targets *in vivo*. MRT-92 drastically reduced the expression of GLI1, which is the best indicator of an active HH pathway. AZD-1775 strongly decreased the phosphorylation of CDC2, a direct target of WEE1 (**Fig. 7F**). In xenograft sections of mice treated with MRT-92+AZD-1775, we observed a significant increase in cleaved caspase 3 expression, consistent with in vitro results (**Fig. 7G** and **H**). Altogether, these results indicate that the coadministration of MRT-92 and AZD-1775 strongly improves the effect of single treatments, nearly abrogating tumor growth.

Discussion

iCCA is an aggressive tumor with a dismal prognosis and limited therapeutic options (1, 4). Prompted by the need for novel and effective treatments, we investigated the role of the HH pathway as a potential therapeutic target for iCCA. Pharmacologic inhibition of SMO reduces iCCA viability and growth. Importantly, the blockade of SMO induces DNA damage and activates the cell-cycle checkpoint WEE1, increasing the vulnerability of iCCA cells to WEE1 inhibition. Hence, targeting WEE1 with AZD-1775 enhanced the efficacy of pharmacologic inhibition of SMO *in vitro* and in an iCCA xenograft model. Our data provide the first evidence that the combination of SMO and WEE1 inhibitors is effective in iCCA and well tolerated *in vivo*, highlighting the translatability of this pharmacologic combination in a clinical setting.

Expression of the HH pathway components SMO, GLI1, and GLI2 was upregulated in iCCA cells compared with that in NHCs. Hyperactivation of the HH pathway was confirmed by the analysis of transcriptomic datasets from surgically resected human iCCA samples, which revealed increased expression of *GLI1, GLI2*, and the target *PTCH1* in the tumor compared with the surrounding nontumor tissue. Overall, these data identified a wide subgroup of patients with CCA that may benefit from pharmacologic targeting of the HH pathway, which has been recently been correlated with poor prognosis and tumor progression in patients with CCA (44).

Mechanistically, we found that the SMO inhibitor MRT-92 induced DNA DSBs in iCCA cells. The subsequent activation of the ATM–CHK2 axis and of the cell-cycle checkpoint kinase WEE1 leads to phosphorylation and inactivation of CDC2, a key regulator of mitotic entry (38), suggesting that iCCA cells are impeded from entering mitosis. Nevertheless, expression of pSer10 Histone H3 indicates that iCCA cells can initiate the very early phases of mitosis, even in the absence of a significant CDC2 activity (45). This results in the accumulation of Cyclin B1, which promotes mitotic arrest in iCCA cells and the consequent activation of the intrinsic apoptotic pathway. Altogether, these data indicate that MRT-92–dependent activation of the ATM–CHK2 checkpoint arrests cells before the finalization of mitosis, leading to programmed mitochondrial cell death (**Fig. 7I**).

An important finding of this study was that targeting WEE1 enhanced the effect of SMO inhibition in reducing iCCA growth *in vitro* and *in vivo*. WEE1 is a critical cell-cycle checkpoint kinase involved in the DNA damage response and cell-cycle regulation. Experimental evidence indicates that WEE1 upregulation exerts protumorigenic activity, making cancer cells less sensitive to genomic instability (37, 43). The WEE1 inhibitor AZD-1775 is currently in phase I and II clinical trials as a single agent or in combination with chemotherapy or targeted therapy for various solid and hematologic tumors, including CCA (46–49). Treatment with the WEE1 inhibitor AZD-1775 potentiated the proapoptotic and antiproliferative effects of MRT-92 in both iCCA cell lines. We also investigated the molecular mechanism underlying the improved efficacy of SMO inhibition observed in combination with WEE1 inhibition. The pharmacologic combination of AZD-1775 and MRT-92 strongly enhanced and anticipated the induction of DNA damage, as indicated by the increased expression of phosphorylated γH2A.X and PARP1 processing. Moreover, combined treatment with SMO and WEE1 inhibitors increased the arrest of cells in the mitotic phase, as indicated by the higher levels of phosphorylated H3 and enhanced accumulation of Cyclin B1. Furthermore, suppressing the activity of WEE1 in MRT-92 treated iCCA cells induced an aberrant mitotic process as a result of the accumulation and worsening of genomic instability in iCCA cells, thus potentiating MRT-92 antiproliferative and proapoptotic

Figure 6.

Pharmacologic inhibition of WEE1 potentiates the effects of SMO blockade in iCCA cells. **A,** Evaluation of cell viability in HuCCT1 and CCLP1 cells treated with DMSO, MRT-92 (0.65 μmol/L), AZD-1775 (0.1 μmol/L), or their combination for 24, 48, and 72 hours. **B,** Evaluation of apoptosis by AnnexinV/7-AAD double staining in HuCCT1 and CCLP1 cells treated with DMSO, MRT-92 (0.65 μmol/L), AZD-1775 (0.1 μmol/L), or their combination for 24 and 48 hours. Early apoptosis is detected by Annexin V+/7-AAD-, late apoptosis by Annexin V+/7-AAD+. **C,** Western blot of GLI1, DNA damage, cell-cycle and apoptotic markers in CCLP1 cells treated with DMSO, MRT-92 (0.65 μmol/L), AZD-1775 (0.1 μmol/L), or their combination for 24 hours. HSP90 was used as loading control. **D,** Immuno-fluorescence of pH3-Ser10 in CCLP1 cells treated with DMSO, MRT-92 (0.65 μmol/L), AZD-1775 (0.1 μmol/L), or their combination for 24 hours. Bar = 30 μm. **E,** Graph reports densitometric quantification of BAX/BCL-2 ratio, as shown in **C**. In **A, B,** and **E,** data are expressed as fold change relative to DMSO, which was equated to 1. Data represent mean ± SD (**A**, **B**) and mean ± SEM (**E**) of at least three independent experiments. *, $P < 0.05$; **, $P < 0.01$; ***, $P < 0.001$; ****, $P < 0.0001$.

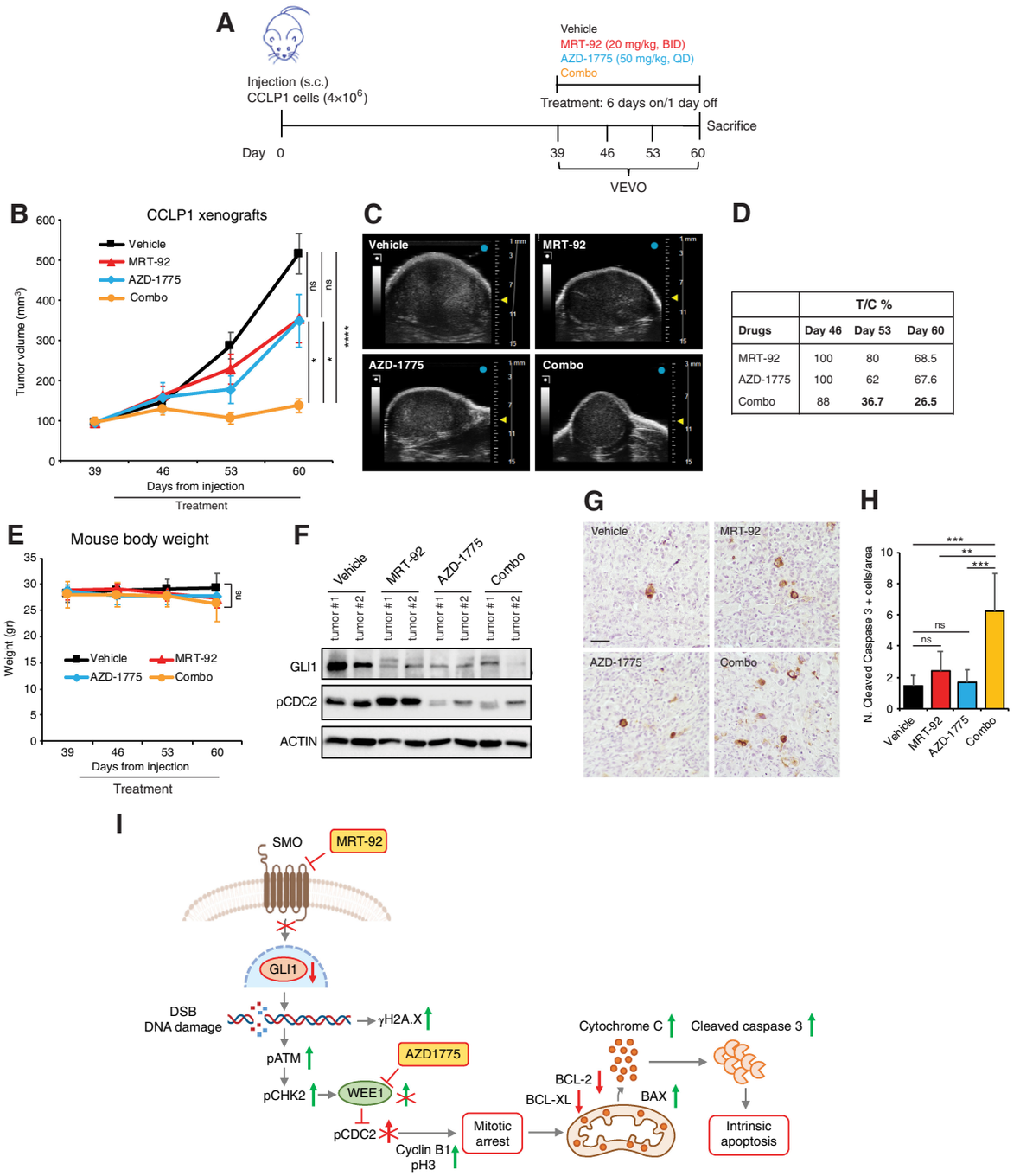

Figure 7.

Combination of SMO and WEE1 inhibitors reduces tumor growth in iCCA xenografts. **A,** Experimental design and treatment timeline. **B,** *In vivo* tumor growth of CCLP1 cells subcutaneously injected into NOD/SCID mice. When tumors reached 100 mm^3 on average, mice were randomized into four groups and treated intraperitoneally with MRT-92 (20 mg/kg, twice a day; $n = 7$), by gavage with AZD-1775 (50 mg/kg, every day) ($n = 7$), a combination of MRT-92 and AZD-1775 ($n = 8$), or vehicle ($n = 7$). Data are presented as the mean ± SEM. *P* values were calculated using Welch ANOVA and Games-Howell test for multiple comparisons. **C,** Ultrasound images of the tumors. **D,** Table shows the percentage of tumor volume reduction in the treated groups compared with the vehicle-treated group (% T/C ratio). **E,** Mouse body weight during treatment. Data are presented as the mean ± SD. **F,** Western blot showing GLI1 and pCDC2 (pY15-CDK1) proteins in CCLP1 xenografts after 72 hours of treatment. ACTIN was used as a loading control. **G,** Expression of cleaved caspase 3 in paraffin sections of CCLP1 xenografts analyzed by IHC. Sections were counterstained with hematoxylin (blue nuclei). Bar = 100 μm. **H,** Quantification of cleaved caspase 3 staining in the four groups, as shown in (**G**). *, $P < 0.05$; **, $P < 0.01$; ***, $P < 0.001$; ****, $P < 0.0001$; ns, not significant. **I,** Representation of the molecular mechanism underlying combined SMO and WEE1 inhibition. Targeting SMO induces DSB DNA damage and activates the ATM–CHK2 axis resulting in WEE1 phosphorylation and activation. Inhibition of WEE1 with AZD-1775 suppresses the inhibitory phosphorylation of CDC2 induced by MRT-92 treatment, resulting in mitotic arrest and mitochondrial cell death.

outcomes. The mechanism of action of MRT-92 in iCCA cells differs from that previously described for melanoma. MRT-92 treatment activates the ATR–CHK1 axis in melanoma cells following single-strand break and does not result in the activation of WEE1 (13). These findings suggest context-dependent mechanisms of DNA damage response. Hence, the induction of WEE1 upon SMO inhibition might be exploited as an alternative combinatorial strategy in other types of cancer.

The *in vitro* effects of MRT-92 and AZD-1775 combination in both iCCA cell lines translated into a striking *in vivo* antitumor activity in CCLP1 xenografts. Despite the activity of the single agents, the combination of MRT-92+AZD-1775 was effective in reducing tumor growth. Importantly, the simultaneous administration of MRT-92+AZD-1775 was well tolerated *in vivo*, as suggested by the lack of any side effects and the absence of significant variation in body weight in mice. Regarding biomarkers of response, we found that AZD-1775 strongly reduced the expression level of pCDC2, WEE1 direct target and a reliable marker of response to WEE1 inhibition (50). MRT-92 treatment drastically reduced the levels of GLI1 protein, the best read-out of an active HH pathway, indicating a good pharmacologic response to SMO inhibition. Surprisingly, we found that AZD-1775 also reduced GLI1 protein level, although the molecular mechanism underlying this modulation remains unclear.

In conclusion, we obtained novel evidence supporting the role of the HH pathway in the growth of iCCA and identified a downstream molecular mechanism involving the cell-cycle checkpoint kinase WEE1 upon pharmacologic inhibition of SMO. The inhibitory effects of the combinatorial treatment with SMO and WEE1 inhibitors investigated in this study set the stage for the exploration of this therapeutic approach in patients with this type of difficult-to-treat cancer.

Authors' Disclosures

L. Duwe reports grants from Dansk Kræftforksningsfond, Horizon 2020 Marie-Curie Co-Fund PhD Fellowship, and Danish Cancer Society Travel; nonfinancial support from ILCA conference participation; and nonfinancial support from EASL conference participation outside the submitted work. F. Marra reports grants from Menarini; personal fees from AstraZeneca, Ipsen, Roche, Eisai/MSD, Intercept, Novo-Nordisk; nonfinancial support from Gilead, Alfa-Wasserman; and personal fees from Novartis outside the submitted work. No disclosures were reported by the other authors.

Authors' Contributions

G. Anichini: Conceptualization, data curation, formal analysis, investigation, writing–original draft, writing–review and editing. **C. Raggi:** Conceptualization, data curation, formal analysis, funding acquisition, investigation, writing–review and editing. **M. Pastore:** Investigation. **L. Carrassa:** Data curation, supervision, investigation, writing–review and editing. **L. Maresca:** Investigation. **E. Crivaro:** Investigation. **T. Lottini:** Data curation, investigation. **L. Duwe:** Data curation, investigation. **J.B. Andersen:** Formal analysis, writing–review and editing. **L. Tofani:** Formal analysis. **L. Di Tommaso:** Data curation. **J.M. Banales:** Resources. **A. Arcangeli:** Resources, funding acquisition. **F. Marra:** Conceptualization, supervision, funding acquisition, writing–review and editing. **B. Stecca:** Conceptualization, data curation, formal analysis, supervision, funding acquisition, investigation, writing–original draft, writing–review and editing.

Acknowledgments

Funding for this work was partially provided by the Italian Foundation of Cancer Research award to C. Raggi (IG23117) and to F. Marra (IG17786), and institutional funding from ISPRO to B. Stecca. C. Raggi, J.B. Andersen, and J.M. Banales are members of the European Network for the Study of Cholangiocarcinoma (ENSCCA) and participate in the COST Action EURO-CHOLANGIO-NET granted by the COST Association (CA18122). L. Duwe was supported by the European Union's Horizon 2020 research and innovation program under the Marie Skłodowska-Curie grant agreement No. 801481. The authors would like to thank Dr. A.J. Demetris (University of Pittsburgh, Pittsburgh, PA) for providing the cholangiocarcinoma cell lines HuCCT1 and CCLP1, and Prof. E. Petricci (Department of Biotechnology, Chemistry and Pharmacy, University of Siena, Siena, Italy) for providing MRT-92.

The publication costs of this article were defrayed in part by the payment of publication fees. Therefore, and solely to indicate this fact, this article is hereby marked "advertisement" in accordance with 18 USC section 1734.

Note

Supplementary data for this article are available at Molecular Cancer Therapeutics Online (http://mct.aacrjournals.org/).

Received May 30, 2022; revised October 24, 2022; accepted December 1, 2022; published first December 2, 2022.

References

1. Banales JM, Marin JJG, Lamarca A, Rodrigues PM, Khan SA, Roberts LR, et al. Cholangiocarcinoma 2020: the next horizon in mechanisms and management. Nat Rev Gastroenterol Hepatol 2020;17:557–88.
2. Gentilini A, Pastore M, Marra F, Raggi C. The role of stroma in cholangiocarcinoma: The intriguing interplay between fibroblastic component, immune cell subsets, and tumor epithelium. Int J Mol Sci 2018;19:2885.
3. Fabris L, Perugorria MJ, Mertens J, Björkström NK, Cramer T, Lleo A, et al. The tumor microenvironment and immune milieu of cholangiocarcinoma. Liver Int 2019;39:63–78.
4. Banales JM, Cardinale V, Carpino G, Marzioni M, Andersen JB, Invernizzi P, et al. Expert consensus document: Cholangiocarcinoma: current knowledge and future perspectives consensus statement from the European Network for the Study of Cholangiocarcinoma (ENS-CCA). Nat Rev Gastroenterol Hepatol 2016;13:261–80.
5. Sicklick JK, Li YX, Melhem A, Schmelzer E, Zdanowicz M, Huang J, et al. Hedgehog signaling maintains resident hepatic progenitors throughout life. Am J Physiol Gastrointest Liver Physiol 2006;290:G859–70.
6. Omenetti A, Popov Y, Jung Y, Choi SS, Witek RP, Yang L, et al. The hedgehog pathway regulates remodeling responses to biliary obstruction in rats. Gut 2008;57:1275–82.
7. Varjosalo M, Taipale J. Hedgehog: functions and mechanisms. Genes Dev 2008;22:2454–72.
8. Wu F, Zhang Y, Sun B, McMahon AP, Wang Y. Hedgehog signaling: from basic biology to cancer therapy. Cell Chem Biol 2017;24:252–80.
9. Sekulic A, Von Hoff D. Hedgehog pathway inhibition. Cell 2016;164:831.
10. Galperin I, Dempwolff L, Diederich WE, Lauth M. Inhibiting hedgehog: an update on pharmacological compounds and targeting strategies. J Med Chem 2019;62:8392–411.
11. Mazumdar T, Devecchio J, Agyeman A, Shi T, Houghton JA. Blocking hedgehog survival signaling at the level of the GLI genes induces DNA damage and extensive cell death in human colon carcinoma cells. Cancer Res 2011;71:5904–14.
12. Agyeman A, Mazumdar T, Houghton JA. Regulation of DNA damage following termination of hedgehog (HH) survival signaling at the level of the GLI genes in human colon cancer. Oncotarget 2012;3:854–68.
13. Pietrobono S, Santini R, Gagliardi S, Dapporto F, Colecchia D, Chiariello M, et al. Targeted inhibition of hedgehog-GLI signaling by novel acylguanidine derivatives inhibits melanoma cell growth by inducing replication stress and mitotic catastrophe. Cell Death Dis 2018;9:142.
14. Tang L, Tan YX, Jiang BG, Pan YF, Li SX, Yang GZ, et al. The prognostic significance and therapeutic potential of hedgehog signaling in intrahepatic cholangiocellular carcinoma. Clin Cancer Res 2013;19:2014–24.
15. El Khatib M, Kalnytska A, Palagani V, Kossatz U, Manns MP, Malek NP, et al. Inhibition of hedgehog signaling attenuates carcinogenesis in vitro and increases necrosis of cholangiocellular carcinoma. Hepatology 2013;57:1035–45.
16. Razumilava N, Gradilone SA, Smoot RL, Mertens JC, Bronk SF, Sirica AE, et al. Noncanonical hedgehog signaling contributes to chemotaxis in cholangiocarcinoma. J Hepatol 2014;60:599–605.

17. Riedlinger D, Bahra M, Boas-Knoop S, Lippert S, Bradtmöller M, Guse K, et al. Hedgehog pathway as a potential treatment target in human cholangiocarcinoma. J Hepatobiliary Pancreat Sci 2014;21:607–15.
18. Kim Y, Kim MO, Shin JS, Park SH, Kim SB, Kim J, et al. Hedgehog signaling between cancer cells and hepatic stellate cells in promoting cholangiocarcinoma. Ann Surg Oncol 2014;21:2684–98.
19. Kiesslich T, Mayr C, Wachter J, Bach D, Fuereder J, Wagner A, et al. Activated hedgehog pathway is a potential target for pharmacological intervention in biliary tract cancer. Mol Cell Biochem 2014;396:257–68.
20. Han C, Demetris AJ, Michalopoulos GK, Zhan Q, Shelhamer JH, Wu T. PPARgamma ligands inhibit cholangiocarcinoma cell growth through p53-dependent GADD45 and p21 pathway. Hepatology 2003;38:167–77.
21. Andersen JB, Spee B, Blechacz BR, Avital I, Komuta M, Barbour A, et al. Genomic and genetic characterization of cholangiocarcinoma identifies therapeutic targets for tyrosine kinase inhibitors. Gastroenterology 2012; 142:1021–31.
22. Pan S, Wu X, Jiang J, Gao W, Wan Y, Cheng D, et al. Discovery of NVP-LDE225, a potent and selective smoothened antagonist. ACS Med Chem Lett 2010;1:130–4.
23. Lauth M, Bergström A, Shimokawa T, Toftgård R. Inhibition of GLI-mediated transcription and tumor cell growth by small-molecule antagonists. Proc Natl Acad Sci USA 2007;104:8455–60.
24. Pietrobono S, Gaudio E, Gagliardi S, Zitani M, Carrassa L, Migliorini F, et al. Targeting noncanonical activation of GLI1 by the SOX2-BRD4 transcriptional complex improves the efficacy of hedgehog pathway inhibition in melanoma. Oncogene 2021;40:3799–814.
25. Hirai H, Iwasawa Y, Okada M, Arai T, Nishibata T, Kobayashi M, et al. Small-molecule inhibition of Wee1 kinase by MK-1775 selectively sensitizes p53-deficient tumor cells to DNA-damaging agents. Mol Cancer Ther 2009;8:2992–3000.
26. Pietrobono S, Anichini G, Sala C, Manetti F, Almada LL, Pepe S, et al. ST3GAL1 is a target of the SOX2-GLI1 transcriptional complex and promotes melanoma metastasis through AXL. Nat Commun 2020;11:5865.
27. Santini R, Vinci MC, Pandolfi S, Penachioni JY, Montagnani V, Olivito B, et al. Hedgehog-GLI signaling drives self-renewal and tumorigenicity of human melanoma-initiating cells. Stem Cells 2012;30:1808–18.
28. Pandolfi S, Montagnani V, Lapucci A, Stecca B. HEDGEHOG/GLI-E2F1 axis modulates iASPP expression and function and regulates melanoma cell growth. Cell Death Differ 2015;22:2006–19.
29. Raggi C, Fiaccadori K, Pastore M, Correnti M, Piombanti B, Forti E, et al. Antitumor activity of a novel fibroblast growth factor receptor inhibitor for intrahepatic cholangiocarcinoma. Am J Pathol 2019;189:2090–101.
30. Raggi C, Factor VM, Seo D, Holczbauer A, Gillen MC, Marquardt JU, et al. Epigenetic reprogramming modulates malignant properties of human liver cancer. Hepatology 2014;59:2251–62.
31. Raggi C, Correnti M, Sica A, Andersen JB, Cardinale V, Alvaro D, et al. Cholangiocarcinoma stem-like subset shapes tumor-initiating niche by educating associated macrophages. J Hepatol 2017;66:102–15.
32. Kurita S, Mott JL, Almada LL, Bronk SF, Werneburg NW, Sun SY, et al. GLI3-dependent repression of DR4 mediates hedgehog antagonism of TRAIL-induced apoptosis. Oncogene 2010;29:4848–58.
33. Hoch L, Faure H, Roudaut H, Schoenfelder A, Mann A, Girard N, et al. MRT-92 inhibits hedgehog signaling by blocking overlapping binding sites in the transmembrane domain of the Smoothened receptor. FASEB J 2015; 29:1817–29.
34. Buonamici S, Williams J, Morrissey M, Wang A, Guo R, Vattay A, et al. Interfering with resistance to smoothened antagonists by inhibition of the PI3K pathway in medulloblastoma. Sci Transl Med 2010;2:51ra70.
35. Swift LH, Golsteyn RM. Genotoxic anti-cancer agents and their relationship to DNA damage, mitosis, and checkpoint adaptation in proliferating cancer cells. Int J Mol Sci 2014;15:3403–31.
36. Sedelnikova OA, Pilch DR, Redon C, Bonner WM. Histone H2AX in DNA damage and repair. Cancer Biol Ther 2003;2:233–5.
37. Smith HL, Southgate H, Tweddle DA, Curtin NJ. DNA damage checkpoint kinases in cancer. Expert Rev Mol Med 2020;22:e2.
38. Geenen JJJ, Schellens JHM. Molecular pathways: targeting the protein kinase Wee1 in cancer. Clin Cancer Res 2017;23:4540–4.
39. Li DW, Yang Q, Chen JT, Zhou H, Liu RM, Huang XT. Dynamic distribution of Ser-10 phosphorylated histone H3 in cytoplasm of MCF-7 and CHO cells during mitosis. Cell Res 2005;15:120–6.
40. Nakayama Y, Yamaguchi N. Role of cyclin B1 levels in DNA damage and DNA damage-induced senescence. Int Rev Cell Mol Biol 2013;305:303–37.
41. Nam AR, Jin MH, Bang JH, Oh KS, Seo HR, Oh DY, et al. Inhibition of ATR increases the sensitivity to WEE1 inhibitor in biliary tract cancer. Cancer Res Treat 2020;52:945–56.
42. Perry JA, Kornbluth S. Cdc25 and Wee1: analogous opposites? Cell Div 2007;2: 12.
43. Ghelli Luserna di Rorà A, Cerchione C, Martinelli G, Simonetti G. A WEE1 family business: regulation of mitosis, cancer progression, and therapeutic target. J Hematol Oncol 2020;13:126.
44. Anichini G, Carrassa L, Stecca B, Marra F, Raggi C. The role of the hedgehog pathway in cholangiocarcinoma. Cancers 2021;13:4774.
45. Pines J, Rieder CL. Restaging mitosis: a contemporary view of mitotic progression. Nat Cell Biol 2001;3:E3–6.
46. Carrassa L, Damia G. DNA damage response inhibitors: Mechanisms and potential applications in cancer therapy. Cancer Treat Rev 2017;60: 139–51.
47. Kong A, Good J, Kirkham A, Savage J, Mant R, Llewellyn L, et al. Phase I trial of WEE1 inhibition with chemotherapy and radiotherapy as adjuvant treatment, and a window of opportunity trial with cisplatin in patients with head and neck cancer: the WISTERIA trial protocol. BMJ Open 2020; 10:e033009.
48. Cuneo KC, Morgan MA, Sahai V, Schipper MJ, Parsels LA, Parsels JD, et al. Dose escalation trial of the Wee1 inhibitor adavosertib (AZD1775) in combination with gemcitabine and radiation for patients with locally advanced pancreatic cancer. J Clin Oncol 2019;37:2643–50.
49. National Cancer Institute (NCI). Molecular analysis for therapy choice (MATCH); Clinical Trial registration NCT02465060; clinicaltrials.gov, 2022.
50. Restelli V, Lupi M, Chilà R, Vagni M, Tarantelli C, Spriano F, et al. DNA damage response inhibitor combinations exert synergistic antitumor activity in aggressive B-cell lymphomas. Mol Cancer Ther 2019;18:1255–64.